EUROPEAN ORGANISATION FOR NUCLEAR RESEARCH

CERN-PPE/96-025
19 February 1996

Measurement of cross-sections and asymmetries in e^+e^- collisions at 130-140 GeV centre-of-mass energy

The OPAL Collaboration

Abstract

Production of events with multihadronic and leptonic final states has been measured in e^+e^- collisions at centre-of-mass energies significantly above the Z^0 mass, using the OPAL detector at LEP. A substantial production rate of radiative $Z^0\gamma$ events was observed, as expected, together with events with less energetic initial-state photons. The cross-sections and leptonic forward-backward asymmetries were measured and compared with Standard Model expectations. In a model-independent fit to the Z^0 lineshape, the hadronic cross-section and lepton asymmetries presented here provide constraints on the size of the γZ^0-interference term which are complementary to those afforded by LEP data accumulated at the Z^0 resonance.

(To be submitted to Physics Letters B)

The OPAL Collaboration

G. Alexander[23], J. Allison[16], N. Altekamp[5], K. Ametewee[25], K.J. Anderson[9], S. Anderson[12], S. Arcelli[2], S. Asai[24], D. Axen[29], G. Azuelos[18,a], A.H. Ball[17], E. Barberio[26], R.J. Barlow[16], R. Bartoldus[3], J.R. Batley[5], G. Beaudoin[18], J. Bechtluft[14], C. Beeston[16], T. Behnke[8], A.N. Bell[1], K.W. Bell[20], G. Bella[23], S. Bentvelsen[8], P. Berlich[10], S. Bethke[14], O. Biebel[14], V. Blobel[8], I.J. Bloodworth[1], J.E. Bloomer[1], P. Bock[11], H.M. Bosch[11], M. Boutemeur[18], B.T. Bouwens[12], S. Braibant[12], R.M. Brown[20], H.J. Burckhart[8], C. Burgard[27], R. Bürgin[10], P. Capiluppi[2], R.K. Carnegie[6], A.A. Carter[13], J.R. Carter[5], C.Y. Chang[17], C. Charlesworth[6], D.G. Charlton[1,b], D. Chrisman[4], S.L. Chu[4], P.E.L. Clarke[15], I. Cohen[23], J.E. Conboy[15], O.C. Cooke[16], M. Cuffiani[2], S. Dado[22], C. Dallapiccola[17], G.M. Dallavalle[2], C. Darling[31], S. De Jong[12], L.A. del Pozo[8], M.S. Dixit[7], E. do Couto e Silva[12], M. Doucet[18], E. Duchovni[26], G. Duckeck[8], I.P. Duerdoth[16], J.E.G. Edwards[16], P.G. Estabrooks[6], H.G. Evans[9], M. Evans[13], F. Fabbri[2], P. Fath[11], F. Fiedler[12], M. Fierro[2], H.M. Fischer[3], R. Folman[26], D.G. Fong[17], M. Foucher[17], H. Fukui[24], A. Fürtjes[8], P. Gagnon[7], A. Gaidot[21], J.W. Gary[4], J. Gascon[18], S.M. Gascon-Shotkin[17], N.I. Geddes[20], C. Geich-Gimbel[3], S.W. Gensler[9], F.X. Gentit[21], T. Geralis[20], G. Giacomelli[2], P. Giacomelli[4], R. Giacomelli[2], V. Gibson[5], W.R. Gibson[13], D.M. Gingrich[30,a], J. Goldberg[22], M.J. Goodrick[5], W. Gorn[4], C. Grandi[2], E. Gross[26], M. Gruwé[8], C. Hajdu[32], G.G. Hanson[12], M. Hansroul[8], M. Hapke[13], C.K. Hargrove[7], P.A. Hart[9], C. Hartmann[3], M. Hauschild[8], C.M. Hawkes[5], R. Hawkings[8], R.J. Hemingway[6], G. Herten[10], R.D. Heuer[8], M.D. Hildreth[8], J.C. Hill[5], S.J. Hillier[1], T. Hilse[10], P.R. Hobson[25], R.J. Homer[1], A.K. Honma[28,a], D. Horváth[32,c], R. Howard[29], R.E. Hughes-Jones[16], D.E. Hutchcroft[5], P. Igo-Kemenes[11], D.C. Imrie[25], M.R. Ingram[16], A. Jawahery[17], P.W. Jeffreys[20], H. Jeremie[18], M. Jimack[1], A. Joly[18], G. Jones[16], M. Jones[6], R.W.L. Jones[8], U. Jost[11], P. Jovanovic[1], J. Kanzaki[24], D. Karlen[6], T. Kawamoto[24], R.K. Keeler[28], R.G. Kellogg[17], B.W. Kennedy[20], J. King[13], J. Kirk[29], S. Kluth[8], T. Kobayashi[24], M. Kobel[10], D.S. Koetke[6], T.P. Kokott[3], S. Komamiya[24], R. Kowalewski[8], T. Kress[11], P. Krieger[6], J. von Krogh[11], P. Kyberd[13], G.D. Lafferty[16], H. Lafoux[21], R. Lahmann[17], W.P. Lai[19], D. Lanske[14], J. Lauber[15], J.G. Layter[4], A.M. Lee[31], E. Lefebvre[18], D. Lellouch[26], J. Letts[2], L. Levinson[26], C. Lewis[15], S.L. Lloyd[13], F.K. Loebinger[16], G.D. Long[17], B. Lorazo[18], M.J. Losty[7], J. Ludwig[10], A. Luig[10], A. Malik[21], M. Mannelli[8], S. Marcellini[2], C. Markus[3], A.J. Martin[13], J.P. Martin[18], G. Martinez[17], T. Mashimo[24], W. Matthews[25], P. Mättig[3], W.J. McDonald[30], J. McKenna[29], E.A. Mckigney[15], T.J. McMahon[1], A.I. McNab[13], F. Meijers[8], S. Menke[3], F.S. Merritt[9], H. Mes[7], J. Meyer[27], A. Michelini[8], G. Mikenberg[26], D.J. Miller[15], R. Mir[26], W. Mohr[10], A. Montanari[2], T. Mori[24], M. Morii[24], U. Müller[3], B. Nellen[3], B. Nijjhar[16], R. Nisius[8], S.W. O'Neale[1], F.G. Oakham[7], F. Odorici[2], H.O. Ogren[12], T. Omori[24], M.J. Oreglia[9], S. Orito[24], M. Palazzo[2], J. Pálinkás[33,d], J.P. Pansart[21], G. Pásztor[32], J.R. Pater[16], G.N. Patrick[20], M.J. Pearce[1], S. Petzold[27], J.E. Pilcher[9], J. Pinfold[30], D.E. Plane[8], P. Poffenberger[28], B. Poli[2], A. Posthaus[3], H. Przysiezniak[30], D.L. Rees[1], D. Rigby[1], M.G. Rison[5], S.A. Robins[13], N. Rodning[30], J.M. Roney[28], A. Rooke[15], E. Ros[8], A.M. Rossi[2], M. Rosvick[28], P. Routenburg[30], Y. Rozen[8], K. Runge[10], O. Runolfsson[8], D.R. Rust[12], R. Rylko[25], E.K.G. Sarkisyan[23], M. Sasaki[24], C. Sbarra[2], A.D. Schaile[8,e], O. Schaile[10], F. Scharf[3], P. Scharff-Hansen[8], P. Schenk[4], B. Schmitt[3], M. Schröder[8], H.C. Schultz-Coulon[10], M. Schulz[8], P. Schütz[3], J. Schwiening[3], W.G. Scott[20], T.G. Shears[16], B.C. Shen[4], C.H. Shepherd-Themistocleous[27], P. Sherwood[15], G.P. Siroli[2], A. Sittler[27], A. Skillman[15], A. Skuja[17], A.M. Smith[8], T.J. Smith[28], G.A. Snow[17], R. Sobie[28], S. Söldner-Rembold[10], R.W. Springer[30], M. Sproston[20], A. Stahl[3], M. Starks[12], K. Stephens[16], J. Steuerer[27], B. Stockhausen[3], D. Strom[19], F. Strumia[8], P. Szymanski[20], R. Tafirout[18], H. Takeda[24], P. Taras[18], S. Tarem[22], M. Tecchio[8], N. Tesch[3], M. Thiergen[10], M.A. Thomson[8], E. von Törne[3], S. Towers[6], M. Tscheulin[10], E. Tsur[23], A.S. Turcot[9], M.F. Turner-Watson[8], P. Utzat[11], R. Van Kooten[12], G. Vasseur[21], M. Verzocchi[10], P. Vikas[18], M. Vincter[28], E.H. Vokurka[16], F. Wäckerle[10], A. Wagner[27], C.P. Ward[5], D.R. Ward[5], J.J. Ward[15], P.M. Watkins[1], A.T. Watson[1], N.K. Watson[7], P. Weber[6], P.S. Wells[8], N. Wermes[3], J.S. White[28], B. Wilkens[10], G.W. Wilson[27], J.A. Wilson[1], T. Wlodek[26], G. Wolf[26],

S. Wotton[11], T.R. Wyatt[16], S. Xella[2], S. Yamashita[24], G. Yekutieli[26], K. Yoshimura[24], V. Zacek[18],

[1]School of Physics and Space Research, University of Birmingham, Birmingham B15 2TT, UK
[2]Dipartimento di Fisica dell' Università di Bologna and INFN, I-40126 Bologna, Italy
[3]Physikalisches Institut, Universität Bonn, D-53115 Bonn, Germany
[4]Department of Physics, University of California, Riverside CA 92521, USA
[5]Cavendish Laboratory, Cambridge CB3 0HE, UK
[6] Ottawa-Carleton Institute for Physics, Department of Physics, Carleton University, Ottawa, Ontario K1S 5B6, Canada
[7]Centre for Research in Particle Physics, Carleton University, Ottawa, Ontario K1S 5B6, Canada
[8]CERN, European Organisation for Particle Physics, CH-1211 Geneva 23, Switzerland
[9]Enrico Fermi Institute and Department of Physics, University of Chicago, Chicago IL 60637, USA
[10]Fakultät für Physik, Albert Ludwigs Universität, D-79104 Freiburg, Germany
[11]Physikalisches Institut, Universität Heidelberg, D-69120 Heidelberg, Germany
[12]Indiana University, Department of Physics, Swain Hall West 117, Bloomington IN 47405, USA
[13]Queen Mary and Westfield College, University of London, London E1 4NS, UK
[14]Technische Hochschule Aachen, III Physikalisches Institut, Sommerfeldstrasse 26-28, D-52056 Aachen, Germany
[15]University College London, London WC1E 6BT, UK
[16]Department of Physics, Schuster Laboratory, The University, Manchester M13 9PL, UK
[17]Department of Physics, University of Maryland, College Park, MD 20742, USA
[18]Laboratoire de Physique Nucléaire, Université de Montréal, Montréal, Quebec H3C 3J7, Canada
[19]University of Oregon, Department of Physics, Eugene OR 97403, USA
[20]Rutherford Appleton Laboratory, Chilton, Didcot, Oxfordshire OX11 0QX, UK
[21]CEA, DAPNIA/SPP, CE-Saclay, F-91191 Gif-sur-Yvette, France
[22]Department of Physics, Technion-Israel Institute of Technology, Haifa 32000, Israel
[23]Department of Physics and Astronomy, Tel Aviv University, Tel Aviv 69978, Israel
[24]International Centre for Elementary Particle Physics and Department of Physics, University of Tokyo, Tokyo 113, and Kobe University, Kobe 657, Japan
[25]Brunel University, Uxbridge, Middlesex UB8 3PH, UK
[26]Particle Physics Department, Weizmann Institute of Science, Rehovot 76100, Israel
[27]Universität Hamburg/DESY, II Institut für Experimental Physik, Notkestrasse 85, D-22607 Hamburg, Germany
[28]University of Victoria, Department of Physics, P O Box 3055, Victoria BC V8W 3P6, Canada
[29]University of British Columbia, Department of Physics, Vancouver BC V6T 1Z1, Canada
[30]University of Alberta, Department of Physics, Edmonton AB T6G 2J1, Canada
[31]Duke University, Dept of Physics, Durham, NC 27708-0305, USA
[32]Research Institute for Particle and Nuclear Physics, H-1525 Budapest, P O Box 49, Hungary
[33]Institute of Nuclear Research, H-4001 Debrecen, P O Box 51, Hungary

[a] and at TRIUMF, Vancouver, Canada V6T 2A3
[b] and Royal Society University Research Fellow
[c] and Institute of Nuclear Research, Debrecen, Hungary
[d] and Depart of Experimental Physics, Lajos Kossuth University, Debrecen, Hungary
[e] and Ludwig-Maximilians-Universität, München, Germany

1 Introduction

Measurements are presented of cross-sections and forward-backward asymmetries in e^+e^- collisions at centre-of-mass energies, $\sqrt{s}$, from 130 to 140 GeV. The data were recorded by the OPAL experiment at LEP in October and November 1995, during the so-called LEP 1.5 run. These are the highest energy e^+e^- collision data yet available and the first at energies well above the Z^0 resonance. Cross-sections were measured and compared with Standard Model expectations, for multihadronic, e^+e^-, $\mu^+\mu^-$ and $\tau^+\tau^-$ final states, as were the forward-backward asymmetries for the leptonic final states.

A feature of e^+e^- collision data at these centre-of-mass energies is a tendency for radiative return to the Z^0. If one or more initial-state radiation photons are emitted which reduce the effective centre-of-mass energy of the subsequent e^+e^- collision, $\sqrt{s'}$, to the region of the Z^0 resonance, the cross-section is greatly enhanced. A separation can be made between these radiative events and non-radiative events for which $\sqrt{s'} \approx \sqrt{s}$. The properties of the radiative data are expected to be similar to those measured in Z^0 decays during the earlier LEP 1 running, modified only by the boost due to recoil against hard initial-state radiation. The non-radiative data are expected to have somewhat different properties, reflecting the substantially increased relative importance of photon-exchange processes above the Z^0 resonance. The similar size of the photon-exchange and Z^0-exchange amplitudes in the non-radiative data at 130-140 GeV allows constraints to be placed on the size of the interference terms between γ and Z^0 amplitudes, complementing the measurements made at the Z^0 resonance.

2 Data and simulation

The OPAL detector is fully described elsewhere [1–4]. The data used in this analysis were recorded at nominal e^+e^- centre-of-mass energies of 130, 136 and 140 GeV. Integrated luminosities of 2.7, 2.6 and 0.04 pb^{-1}, respectively, were included in the analysis from the three energy points. The average centre-of-mass energies of the e^+e^- system were estimated to be 130.26 GeV and 136.23 GeV during the nominal 130 and 136 GeV data-taking periods [5], with a common systematic uncertainty of 0.06 GeV. Since the luminosity collected at 140 GeV was very low the analysis at that centre-of-mass energy is not discussed in any detail, but cross-sections are quoted where the statistics permit.

For Monte Carlo simulation studies of $e^+e^- \to$ hadrons we used the PYTHIA [6] program with input parameters optimized by a study of global event shape variables and particle production rates in Z^0 decay data [7]. For $e^+e^- \to e^+e^-$ we used the BABAMC [8] Monte Carlo program and for $e^+e^- \to \mu^+\mu^-$ and $e^+e^- \to \tau^+\tau^-$ the KORALZ program [9]. Two-photon background processes were simulated using PYTHIA at low Q^2 and TWOGEN [10] at high Q^2, and background from the process $e^+e^- \to \gamma\gamma$ using the RADCOR [11] program. All samples were processed through the OPAL detector simulation program [12].

3 Measurement of the luminosity

The luminosity recorded by the OPAL detector was measured using small-angle Bhabha scattering, $e^+e^- \to e^+e^-$, in the forward calorimetry. Independent measurements were available from two separate devices: a high precision silicon-tungsten luminometer, covering angles from the beam between 25 and 59 mrad, and a lead-scintillator sampling calorimeter instrumented with streamer tubes, covering the region from 40 to 150 mrad.

The silicon-tungsten luminometer [4] consists of two finely segmented silicon tungsten calorimeters placed around the beam pipe, symmetrically on the left and right sides of the OPAL detector, 2.4 m

away from the interaction point. Each calorimeter is composed of a stack of 19 silicon wafers interspersed with 18 tungsten plates. The sensitive area of each silicon wafer extends from 62 to 142 mm from the beam axis and is segmented into 32 pads radially and 32 in azimuth around the beam. The radial position of electron showers in the calorimeter can be determined with very little systematic uncertainty, allowing a luminosity measurement of 0.1% precision to be achieved [13]. A simpler analysis is reported here since such a precise luminosity measurement is not needed. Furthermore, the acceptance of the luminometer was reduced at the trigger level by a prescaling factor of 16 in order to increase the experimental live time as far as possible.

Bhabha scattering events were selected by requiring a high energy cluster in each end of the detector, using asymmetric acceptance cuts. The inner and outer radial acceptance cuts delimited a region between 31 and 52 mrad on one side of the calorimeter, while for the opposite calorimeter a wider zone between 27 and 56 mrad was used. Two luminosity measurements were formed with the narrower acceptance on one or the other side. The final measurement was the average of the two and has no first-order dependence on beam offsets or tilts. The relative error on the luminosity measurement obtained was 1.0%, dominated by the statistics of the data (0.9%). The principal systematic uncertainties were Monte Carlo statistics (0.25%) and theoretical knowledge of the cross-section (0.25%). The Monte Carlo program BHLUMI 4.02a was used for calculating the Bhabha cross-section at these energies [14].

The acceptance of the larger forward detector was lower than in previous publications because of the addition of the silicon-tungsten luminometer on the inside front edge of the device. The selection of Bhabha events within the calorimeter acceptance was similar to that used in previous publications [15–17]. For this analysis, however, the overall acceptance of the calorimeter was measured by normalizing to the precisely known cross-section for hadronic events at the Z^0 peak, using LEP 1 data collected earlier in 1995. Small corrections were derived from Monte Carlo simulations [14], using observed detector resolutions, to reflect small changes in the detector acceptance between 91 GeV and 130-140 GeV centre-of-mass energies. The main sources of systematic uncertainty on the luminosity measured in the forward detector arose from the knowledge of the multihadron acceptance for the 1995 LEP 1 data and the energy dependence of the forward detector acceptance. A total systematic uncertainty of 0.8% was estimated, which together with a 0.6% statistical error gives a total luminosity uncertainty from the forward detector of 1.0%.

The luminosity measurements from the silicon-tungsten luminometer and from the forward detector are consistent, differing by (1.8±1.3)%. The mean of the luminosity measurements from the two devices was used in this analysis and a total luminosity error of 1.0% was applied, which is small compared to the statistical uncertainties on the other event samples. A further check was made using Bhabha scattering events recorded within the electromagnetic calorimeter, as described in section 5. Using events within the region $|\cos\theta| < 0.96$, where θ is the polar angle relative to the e^- beam direction, the luminosity measurements have been checked with a precision of 2.6%.

4 Hadronic events

Hadronic events were selected from the data using the same criteria as in earlier OPAL studies of hadronic Z^0 decays [17]. Although these criteria have not been optimized for the higher energy data, studies using the PYTHIA Monte Carlo program show that they have an efficiency at $\sqrt{s} = 130$ GeV of (96.6±0.2)% and at $\sqrt{s} = 136$ GeV of (96.1±0.2)% for events with $s'/s > 0.01$, with a bias between radiative and non-radiative events of less than 3%. The cut on visible energy was tightened from $0.10\sqrt{s}$ to $0.14\sqrt{s}$ in order to reduce the background from two-photon processes from 4.7% to (2.6±0.9)%, with a further loss in efficiency of 1.3% at $\sqrt{s} = 130$ GeV and 1.6% at $\sqrt{s} = 136$ GeV. The numbers of events selected using these cuts at the three centre-of-mass energy points are shown in table 1, together with the corresponding cross-sections.

The effective centre-of-mass energy, $\sqrt{s'}$, of the e^+e^- collision was estimated for each hadronic event as follows. The "Durham" jet finding scheme [20] was used to form the particles into two jets with polar angles θ_1 and θ_2. The energy of a possible undetected initial-state photon along the beam direction was estimated, assuming massless three-body kinematics, as $\sqrt{s} \cdot |\sin(\theta_1+\theta_2)|/(|\sin(\theta_1+\theta_2)| + \sin\theta_1 + \sin\theta_2)$. An alternative procedure was to use the measured energy and momentum by performing a kinematic fit to a system of jets and an unmeasured photon along the beam direction, imposing constraints of energy and momentum conservation. The two procedures were found to yield very similar results. However, in approximately 20% of radiative events the photon was detected directly in the electromagnetic calorimeter. Such photons were identified by requiring them to conform to the expected transverse shower shape and to be isolated by observing no more than 1 GeV in a cone of half-angle 200 mrad. The photon energy, E_γ, was derived from the event kinematics or the energy found in the calorimeter, whichever was the larger, and was used to compute $s' = s - 2E_\gamma\sqrt{s}$. The typical resolution on $\sqrt{s'}$ is ~ 3 GeV.

The distribution of $\sqrt{s'}$ estimated in this way, uncorrected for resolution, is shown in figures 1(a) and (b) for 130 and 136 GeV centre-of-mass energy, respectively. For comparison, the predictions of PYTHIA are superimposed. By making a cut on this distribution the cross-section for the "non-radiative" events, with only a little initial-state radiation, can be derived. This sample was defined by $s'/s > 0.8$; in figures 1(a) and (b) the Monte Carlo contribution having the generated value of $s'/s > 0.8$ is shaded. The selection has an efficiency of approximately 84% for events with true $s'/s > 0.8$, a background from events with $s'/s < 0.8$ of approximately 12%, and a residual background from other processes of 3%. The mean effective centre-of-mass energy in the non-radiative 130 and 136 GeV samples, estimated from PYTHIA, was found to be approximately 129 and 134 GeV, respectively, rather close to the full centre-of-mass energy. The measured non-radiative cross-sections, after correction for acceptance and resolution, are shown in table 1. The total and non-radiative cross-sections are shown in figure 2 and compared to the Standard Model expectations which are shown as solid curves. The uncertainty on the cross-sections is dominated by the statistics of the selected multihadron samples ($> 3\%$ in all cases), with systematic contributions from the luminosity uncertainty (1.0%) and the multihadron selection. The main systematic uncertainties in the selection of the inclusive sample (total systematic error 1.4%) come from the knowledge of the two-photon background contamination (0.9%) and from detector stability (1.0%). In the non-radiative sample, systematic uncertainties arise from the modelling of the separation of the radiative and non-radiative events, estimated to be at the level of 4% by comparing different separation methods (3%) and different Monte Carlo initial-state radiation treatments (2%). In both the total and non-radiative samples the measured cross-sections are in agreement with the Standard Model predictions, with the 130 GeV non-radiative cross-section showing the largest deviation, being two standard deviations below the expectation.

5 e^+e^- final state

Events containing e^+e^- in the final state were selected following [15]. In particular, the acollinearity angle, $\theta_{\rm acol}$, between the electrons was required to satisfy $\theta_{\rm acol} < 10^\circ$, which corresponds quite closely to the $s'/s > 0.8$ cut used for the hadronic channel for the angular region considered here. The total numbers of events selected with the observed electron within the polar angle range $|\cos\theta_{e^-}| < 0.7$ are shown in table 1 for centre-of-mass energies of 130 and 136 GeV, together with the corresponding cross-sections. They are compared with the predictions of the ALIBABA [19] program in figure 2. The systematic uncertainty on the electron acceptance was estimated to be 1.2%, dominated by the knowledge of inefficiencies in the selection, primarily from the association of a charged track with an electromagnetic cluster. To increase the acceptance for radiative events in the central part of the detector a second sample was selected by loosening the acollinearity cut to $\theta_{\rm acol} < 90^\circ$ and requiring that both electron and positron be observed within $|\cos\theta| < 0.7$. The cut on the sum of

Channel	$\sqrt{s}$ (GeV)	Selected events	σ (pb)	σ^{SM} (pb)
Hadrons ($s'/s > 0.01$)	130.26	819	315±11±5	330
	136.23	658	261±11±4	274
	140	11	281±91±4	246
Hadrons ($s'/s > 0.8$)	130.26	177	66±5±3	78
	136.23	155	60±5±2	63
	140	2	50±36±2	56
$\mathrm{e^+e^-}(\lvert\cos\theta_{\mathrm{e^-}}\rvert < 0.7, \theta_{\mathrm{acol}} < 10^\circ)$	130.26	110	41.7±4.0±0.7	41.6
$\mathrm{e^+e^-}(\lvert\cos\theta_{\mathrm{e^-}}\rvert < 0.7, \theta_{\mathrm{acol}} < 10^\circ)$	136.23	96	38.0±3.9±0.6	38.2
$\mathrm{e^+e^-}(\lvert\cos\theta\rvert < 0.7, \theta_{\mathrm{acol}} < 90^\circ)$	130.26	135	50.6±4.4±0.8	50.7
$\mathrm{e^+e^-}(\lvert\cos\theta\rvert < 0.7, \theta_{\mathrm{acol}} < 90^\circ)$	136.23	112	43.8±4.2±0.7	45.9
$\mathrm{e^+e^-}(\lvert\cos\theta\rvert < 0.96, \theta_{\mathrm{acol}} < 10^\circ)$	130.26	1670	617±16±13	645
$\mathrm{e^+e^-}(\lvert\cos\theta\rvert < 0.96, \theta_{\mathrm{acol}} < 10^\circ)$	136.23	1505	582±16±13	596
$\mathrm{e^+e^-}(\lvert\cos\theta\rvert < 0.96, \theta_{\mathrm{acol}} < 10^\circ)$	140	25	730±150±80	564
$\mu^+\mu^-(s'/s > 0.01)$	130.26	55	23.0±3.1±0.4	22.1
$\mu^+\mu^-(s'/s > 0.01)$	136.23	55	23.9±3.2±0.5	18.9
$\mu^+\mu^-(s'/s > 0.8)$	130.26	26	9.5±1.9±0.2	8.2
$\mu^+\mu^-(s'/s > 0.8)$	136.23	30	11.6±2.1±0.2	7.1
$\tau^+\tau^-(s'/s > 0.01)$	130.26	24	24.3±5.0±0.6	22.1
$\tau^+\tau^-(s'/s > 0.01)$	136.23	25	27.1±5.4±0.6	18.9
$\tau^+\tau^-(s'/s > 0.8)$	130.26	9	6.0±2.0±0.2	8.2
$\tau^+\tau^-(s'/s > 0.8)$	136.23	11	7.6±2.3±0.2	7.1

Table 1: Numbers of selected events and measured cross-sections. The first error shown is statistical and the second is systematic. The σ^{SM} values shown are the Standard Model predictions from the ZFITTER [18] (hadrons, $\mu^+\mu^-$, $\tau^+\tau^-$) and ALIBABA [19] ($\mathrm{e^+e^-}$) programs. Note that the measured cross-sections are corrected to the phase-space limit imposed by the s'/s cut with s' defined as the invariant mass of the outgoing two-fermion system *before* final-state photon radiation. There is a small ambiguity associated with this definition, coming from the effect of interference between initial- and final-state radiation, but this is estimated to be negligible compared to the precision of the measurements. For example, the effect of this interference is estimated to be $\leq$1 pb on the hadronic non-radiative cross-sections.

electromagnetic energy as a fraction of the centre-of-mass energy was also changed from 0.8 to 0.6 for this looser selection. The $\sqrt{s'}$ distributions observed in this sample, calculated using massless three-body kinematics as described in the previous section, are shown in figures 1(c) and (d), together with the predictions of ALIBABA. The cross-sections measured from this sample are given in table 1.

At these energies the production of $\mathrm{e^+e^-}$ is dominated by the QED t-channel Bhabha scattering process, giving a strongly forward-peaked distribution in $\cos\theta_{\mathrm{e^-}}$. Nonetheless, forward-backward asymmetries can be determined and compared with those measured at centre-of-mass energies near the $\mathrm{Z^0}$ mass, where the t-channel is less prominent. The asymmetries were evaluated by counting the numbers of events in the forward and backward $\cos\theta_{\mathrm{e^-}}$ hemispheres. The asymmetries in the region $\lvert\cos\theta_{\mathrm{e^-}}\rvert < 0.7$, $\theta_{\mathrm{acol}} < 10^\circ$, were 0.80±0.06±0.02 and 0.75±0.07±0.02 at 130 and 136 GeV, respectively, where the errors are statistical and systematic. The average of these values over the two energies is 0.78±0.04±0.02 (mean centre-of-mass energy 132.8 GeV). This is compared with measurements at the $\mathrm{Z^0}$ resonance and with the predictions of ALIBABA [19] in figure 3(a). Figure 3(c) shows the angular distribution of the scattered electron compared with the expectation from ALIBABA.

A further selection of $\mathrm{e^+e^-}$ events has been made over the extended range $\lvert\cos\theta\rvert < 0.96$, which is

expected to be even more dominated by the t-channel process. For this selection it was required that the summed electromagnetic energy scaled by the centre-of-mass energy be larger than 0.7, that both e^+ and e^- satisfy $|\cos\theta| < 0.96$ and that $\theta_{\rm acol} < 10^\circ$. Further, explicit requirements that there be charged tracks reconstructed in the event were dropped, thus avoiding acceptance uncertainties from the modelling of the fraction of electromagnetic showers which start before or within the tracking chambers. This is more of a problem in the endcap regions of the detector, because more material is traversed than in the barrel acceptance. The selection therefore included $(3.1\pm0.1)\%$ background from the $\gamma\gamma$ final state. The main systematic uncertainty in the selection arises from how well the edge of the acceptance is modelled. This was checked by comparing the polar angles measured from the electromagnetic calorimeter cluster position with the reconstructed central detector track direction, where such a track was found. Based on this study an uncertainty of 0.8% in the measured cross-section was estimated. The total systematic error on this electron selection is 1.3%. The observed numbers of events and cross-sections are listed in table 1, corrected for the main background from the $\gamma\gamma$ final state [11]. The expected cross-sections at the three energies are also given in the table. The good agreement between data and predictions provides a further consistency check of the measured luminosity.

6 $\mu^+\mu^-$ and $\tau^+\tau^-$ final states

The selection of $\mu^+\mu^-$ events followed that described in previous publications [15] and was estimated to have an efficiency of $(82.8\pm0.3)\%$ at $\sqrt{s}$ =130 GeV and $(81.8\pm0.3)\%$ at $\sqrt{s}$ =136 GeV, for events with $s'/s > 0.01$. The value of s' was estimated event-by-event from the polar angles of the two muons relative to the beam axis, as for the hadronic events. The distributions of $\sqrt{s'}$ obtained are shown in figures 1(e) and (f) for the 130 and 136 GeV data, respectively. The residual background in the sample was estimated to be $(8.2\pm1.4)\%$ at $\sqrt{s}$ =130 GeV and $(9.5\pm1.7)\%$ at 136 GeV, almost all from two-photon scattering processes. A non-radiative event sample was selected by requiring that the reconstructed s' satisfy $s'/s > 0.8$. The absolute efficiency of the selection of non-radiative events with true $s'/s > 0.8$ was estimated to be $(91.5\pm0.3)\%$ at 130 GeV and $(90.8\pm0.3)\%$ at 136 GeV. The residual background in the sample from other channels was estimated to be $(1.6\pm0.2)\%$, all τ-pairs. The residual background from $\mu^+\mu^-$ events with lower s'/s values was estimated to be approximately 10%. The numbers of selected events and the cross-sections derived are shown in table 1. The measured cross-sections are compared with the predictions of the ZFITTER program [18] in figure 2. There is reasonable agreement. Statistical errors dominate the experimental precision. The main sources of systematic error come from the luminosity measurement and the limited Monte Carlo statistics available to evaluate both the acceptance and the background.

The forward-backward asymmetry was evaluated from the measured $\cos\theta$ of the μ^- using a counting method. Monte Carlo events were used to correct for efficiency and background, including feed-through of muon pair events with lower s'/s into the non-radiative sample. The asymmetries obtained, corrected to full acceptance and averaged over the two energies, are 0.28 ± 0.09 for the inclusive sample, and 0.65 ± 0.12 for the $s'/s > 0.8$ sample. These results are shown in figure 3(b), where they are compared with the values measured at the Z^0 resonance and with the Standard Model expectations. The distribution of $\cos\theta$ for the μ^- in the non-radiative sample is shown in figure 3(d), illustrating the substantial asymmetry.

An inclusive sample of $\tau^+\tau^-$ events was selected using the cuts described in [17] after loosening the acollinearity cut to $\theta_{\rm acol} < 60^\circ$, and, in addition, requiring a large visible energy in the event and a large missing transverse momentum relative to the beam axis. The total visible energy in the event was required to exceed $0.3\sqrt{s}$. Requirements were placed on the magnitude and direction of the reconstructed missing momentum vectors. The magnitude of the vector sum of the transverse momenta of the charged tracks and calorimeter clusters in the event, $p_t^{\rm miss}$, was required to exceed $0.08\sqrt{s}$. This

sum was re-evaluated using only calorimeter clusters and required to exceed $0.04\sqrt{s}$. The polar angles, θ, of the two missing momentum vectors with respect to the beam direction, evaluated firstly using only charged tracks and secondly only calorimeter clusters, were both required to satisfy $|\cos\theta| < 0.95$. These extra requirements were found to reduce substantially the large background from two-photon processes. The absolute efficiency of the selection was estimated to be (35.8±0.3)% at 130 GeV and (34.9±0.4)% at 136 GeV, for events with $s'/s > 0.01$. The residual background in the sample was estimated to be (3.6±1.8)%, almost all from two-photon scattering processes. The numbers of selected events and corresponding measured cross-sections are shown in table 1, and the distributions of $\sqrt{s'}$, reconstructed from the τ directions, as for the other channels, are shown in figures 1(g) and (h).

The background from two-photon processes to $\tau^+\tau^-$ events with $s'/s > 0.8$ is much less problematic than for the inclusive sample, since the signal events are more collinear. The selection of the non-radiative sample was therefore able to proceed with less modification to the criteria of [17]: the only changes were that the total visible energy cut was raised to $0.35\sqrt{s}$ and a missing momentum cut, $p_t^{\rm miss} > 0.08\sqrt{s}$, was applied. The absolute efficiency of the selection was estimated to be (49.6±0.6)% at 130 GeV and (50.7±0.8)% at 136 GeV, for events with true $s'/s > 0.8$. The residual background in the sample from other channels was (4.8±2.2)%, and the background from lower s'/s approximately 7%. The corresponding measured cross-sections are shown in table 1 and figure 2.

The forward-backward asymmetry was measured in these τ-pair events using a counting method, correcting for acceptance and background as for the muon-pair events. The result in the inclusive sample, averaging over the 130 and 136 GeV data, is 0.31±0.16, consistent with Standard Model expectations. The observed $\cos\theta_{\tau^-}$ distribution in the non-radiative sample is shown in figure 3(e). It is evident that all the selected events in the data have $\cos\theta_{\tau^-} > 0$, so that the asymmetry of the observed events is unity. This would translate into a larger, unphysical, corrected asymmetry if the usual procedure were adopted. To assess whether the observed forward-backward division of events is consistent with Standard Model expectations a comparison was instead made at the level of observed events. In the forward hemisphere 17.4±0.6 events are expected from signal and background combined, and 19 observed, while in the backward hemisphere 4.3±0.5 are expected and none observed, taking the Standard Model prediction for the asymmetry. Given this expectation, the probability of obtaining no events in the backward hemisphere is 1.5%.

Combined asymmetries from the $\mu^+\mu^-$ and $\tau^+\tau^-$ channels were obtained, assuming μ-τ universality, by forming a weighted average of the corrected numbers of forward and backward events observed in the two channels. A combined asymmetry of 0.29±0.08 was obtained for the sample with $s'/s > 0.01$ and 0.73±0.09 for $s'/s > 0.8$.

7 Influence on precise electroweak measurements

The cross-section and asymmetry measurements presented in this paper are all consistent with the Standard Model expectations, as illustrated in figures 2 and 3 and table 1. The non-radiative data can be used to constrain the size of the interference terms between photon-exchange and Z^0-exchange processes, which have amplitudes of similar magnitude at $\sqrt{s'}$ = 130-140 GeV.

In previous publications by OPAL [15–17], and the other LEP collaborations [21], LEP 1 cross-section and forward-backward asymmetry data, recorded at centre-of-mass energies within a few GeV of the Z^0 mass, have been used to fit the Z^0 lineshape and determine standard electroweak parameters such as the mass, m_Z, and width, Γ_Z, of the Z^0 resonance. The hadronic γZ^0-interference term has normally been kept fixed in these lineshape fits to the value expected within the Standard Model. An alternative, model-independent fitting technique follows the S-matrix approach, developed in [22,23]

and used in [24, 25]. The size of the hadronic γZ^0-interference term is given by the j^{tot}_{had} parameter[1]. In the Standard Model $j^{tot}_{had} = 0.22$, for a top quark mass of 180 GeV and a Higgs mass of 300 GeV. Allowing j^{tot}_{had} to vary freely in a fully model-independent fit leads to only a poor constraint on j^{tot}_{had} and a large negative correlation between j^{tot}_{had} and m_Z, resulting in a significantly larger uncertainty on m_Z than when the interference term is fixed [24,26]. The error can be reduced by including in the lineshape fit cross-section measurements made at centre-of-mass energies far away from the Z^0 resonance, as has recently been done by the TOPAZ Collaboration [25] using data recorded at $\sqrt{s} = 57.77$ GeV.

We have performed Z^0 lineshape fits to OPAL data, using the ZFITTER [18] and SMATASY [23] programs, in which the hadronic γZ^0-interference term has been left free. The results for j^{tot}_{had} and m_Z are given in table 2. The first fit used only LEP 1 data, recorded by OPAL between 1989 and 1992 [15–17] and consisting of a total integrated luminosity of approximately 47 pb^{-1}, with 9 pb^{-1} acquired at off-peak centre-of-mass energy points within ± 3 GeV of m_Z. The second fit included also the LEP 1.5 measurements of non-radiative hadronic cross-sections at energies of 130 and 136 GeV as presented in this paper. The LEP 1.5 data significantly improve the precision of the measurement of j^{tot}_{had}, and also reduce the error on m_Z and the correlation of j^{tot}_{had} and m_Z, as illustrated in figure 4. The fitted value of j^{tot}_{had} including the LEP 1.5 data is seen to lie approximately two standard deviations below the Standard Model prediction, following from the slightly lower than expected non-radiative hadronic cross-sections observed (table 1). The fitted value of m_Z obtained when j^{tot}_{had} is fixed at its Standard Model value is $m_Z = 91.181 \pm 0.009$ GeV. When the analysis of the full LEP 1 data sample is completed, the error on m_Z from the Standard Model fit should be significantly reduced.

The dependence of lepton-pair forward-backward asymmetries on centre-of-mass energy near to m_Z is determined by the size of the leptonic γZ^0-interference term in the cross-section. As can be seen from figure 3(b), the energy-dependence of the leptonic forward-backward asymmetry changes for $\sqrt{s} > 110$ GeV. At $\sqrt{s} =$ 130-140 GeV the size, rather than the energy-dependence, of the non-radiative asymmetry is determined almost entirely by the leptonic γZ^0-interference term. In the S-matrix approach this is given by the j^{fb}_{ℓ} parameter[2]. In the Standard Model $j^{fb}_{\ell} = 0.799$, for a top quark mass of 180 GeV and a Higgs mass of 300 GeV. Table 2 gives the values of j^{fb}_{ℓ} extracted from OPAL data. The first fit used only LEP 1 data from 1989 to 1992 [15–17]. The second fit included also the LEP 1.5 non-radiative forward-backward asymmetry extracted from the combined $\mu^+\mu^-$ and $\tau^+\tau^-$ samples. The LEP 1.5 data give a more precise determination of j^{fb}_{ℓ}, and a central value which is consistent with the Standard Model prediction at the level of 1.7 standard deviations. The uncertainties on other electroweak parameters determined by the different fitting procedures are very little affected by the inclusion of these high-energy data.

Between 1993 and 1995 OPAL recorded a further 125 pb^{-1} of LEP 1 data, of which more than 36 pb^{-1} were at two off-peak centre-of-mass energy points approximately 1.8 GeV above and below m_Z. These data are still being analysed but will give increased sensitivity to the size of the γZ^0-interference terms, particularly j^{fb}_{ℓ}. The uncertainty on j^{tot}_{had} will not improve greatly when adding the additional off-peak data because they were collected at only two off-peak energy points. Using all OPAL LEP 1 data, the final errors on m_Z, j^{tot}_{had} and j^{fb}_{ℓ} are expected to be approximately ± 0.010 GeV, ± 0.60, and ± 0.023, respectively, from this S-matrix approach. Combination of these data with the LEP 1.5 data can be expected to reduce these m_Z and j^{tot}_{had} errors to ± 0.008 GeV and ± 0.40 respectively, with no significant change to the j^{fb}_{ℓ} error. The LEP 1.5 data will therefore continue to provide a useful further constraint on j^{tot}_{had} compared to that from the LEP 1 data alone.

[1] The parameter j^{tot}_{had} is equal to j_T^{had}, as defined by equation (43) in reference [23]. The parameters j^{had}_{tot}, used in [24], and J_{had}, used in [25], are also equal to j^{tot}_{had}.

[2] The parameter j^{fb}_{ℓ} is equal to $\frac{4}{3} j^{\ell}_{FB}$, as defined by equation (43) in reference [23]. In previous OPAL publications [15–17] we have used $C^a_{\gamma Z}$ to parametrize this leptonic interference term. The approximate relationship is $C^a_{\gamma Z} = 0.313 j^{fb}_{\ell}$. A more general conversion between the two parametrizations is discussed in section 3.2 of [23]. Note, however, that $C^a_{\gamma Z}$ and the other C-parameters, as defined in [23], are a factor of 4 smaller than those used by OPAL.

OPAL data sample	j^{tot}_{had}	m_Z (GeV)	j^{tot}_{had}, m_Z correlation	j^{fb}_ℓ
LEP 1 (1989-92) [15–17]	-0.18 ± 0.68	91.187 ± 0.013	-0.70	0.684 ± 0.053
LEP 1 (1989-92) + LEP 1.5	-0.53 ± 0.41	91.192 ± 0.011	-0.50	0.717 ± 0.048

Table 2: Fitted values of the hadronic γZ^0-interference parameter, j^{tot}_{had}, the Z^0 mass, m_Z, and the leptonic γZ^0-interference parameter, j^{fb}_ℓ, using different OPAL data samples. The m_Z values are quoted for the s-dependent Z^0-width.

8 Conclusions

Production of events with multihadronic and leptonic final states has been measured in e^+e^- collisions at centre-of-mass energies significantly above the Z^0 mass. The measured values are all consistent with the Standard Model expectations. In model-independent fits the hadronic cross-section and leptonic forward-backward asymmetries presented here provide complementary constraints on the size of the γZ^0-interference term compared to those afforded by LEP 1 data. The results presented are consistent with those recently reported by the L3 Collaboration [27].

Acknowledgements

We would particularly like to thank the SL Division for the excellent start-up and performance of the short LEP 1.5 data taking run, the precise information on the absolute energy, and their continuing close cooperation with our experimental group. In addition to the support staff at our own institutions we are pleased to acknowledge the
Department of Energy, USA,
National Science Foundation, USA,
Particle Physics and Astronomy Research Council, UK,
Natural Sciences and Engineering Research Council, Canada,
Israel Ministry of Science,
Israel Science Foundation, administered by the Israel Academy of Science and Humanities,
Minerva Gesellschaft,
Japanese Ministry of Education, Science and Culture (the Monbusho) and a grant under the Monbusho International Science Research Program,
German Israeli Bi-national Science Foundation (GIF),
Direction des Sciences de la Matière du Commissariat à l'Energie Atomique, France,
Bundesministerium für Bildung, Wissenschaft, Forschung und Technologie, Germany,
National Research Council of Canada,
Hungarian Foundation for Scientific Research, OTKA T-016660, and OTKA F-015089.

References

[1] OPAL Collab., K. Ahmet et al., Nucl. Instrum. Methods A305 (1991) 275.

[2] P.P. Allport et al., Nucl. Instrum. Methods A324 (1993) 34.

[3] P.P. Allport et al., Nucl. Instrum. Methods A346 (1994) 476.

[4] B.E. Anderson et al., IEEE Transactions on Nuclear Science, 41 (1994) 845.

[5] The LEP energy working group, private communication.

[6] T. Sjöstrand, PYTHIA 5.6 and JETSET 7.3: Physics and Manual, CERN-TH.6488/92;
T. Sjöstrand and M. Bengtsson, Comput. Phys. Commun. 43 (1987) 367;
T. Sjöstrand, Comput. Phys. Commun. 39 (1986) 347.

[7] OPAL Collab., G. Alexander et al., *A comparison of b and uds quark jets to gluon jets*, CERN-PPE/95-126, to be published by Z. Phys. C.

[8] M. Böhm, A. Denner and W. Hollik, Nucl. Phys. B304 (1988) 687;
F.A. Berends, R. Kleiss and W. Hollik, Nucl. Phys. B304 (1988) 712.

[9] S. Jadach et al., Comput. Phys. Commun. 66 (1991) 276.

[10] A. Buijs et al., Comput. Phys. Commun. 79 (1994) 523.

[11] F.A. Berends and R. Kleiss, Nucl. Phys. B186 (1981) 22.

[12] J. Allison et al., Nucl. Instrum. Methods A317 (1992) 47.

[13] J. Hart, in proceedings of *Results and perspectives in Particle Physics*, Les Rencontres de Physique de la Vallée d'Aosta, Editions Frontières, 1994.

[14] S. Jadach, E. Richter-Wąs, B.F.L. Ward and Z. Wąs, Comput. Phys. Commun. 70 (1992) 305;
S. Jadach, E. Richter-Wąs, B.F.L. Ward and Z. Wąs, BHLUMI version 4.02a, unpublished (1995), available from `http://hpjmiady.ifj.edu.pl`.

[15] OPAL Collab., R. Akers et al., Z. Phys. C61 (1994) 19.

[16] OPAL Collab., P.D. Acton et al., Z. Phys. C58 (1993) 219.

[17] OPAL Collab., G. Alexander et al., Z. Phys. C52 (1991) 175.

[18] D. Bardin et al., CERN-TH 6443/92 (May 1992); Phys. Lett. B255 (1991) 290; Nucl. Phys. B351 (1991) 1; Z. Phys. C44 (1989) 493.

[19] W. Beenakker et al., Nucl. Phys. B349 (1991) 323.

[20] S. Catani et al., Phys. Lett. B269 (1991) 432;
N. Brown and W.J. Stirling, Z. Phys. C53 (1992) 629;
S. Bethke, Z. Kunszt, D. Soper and W.J. Stirling, Nucl. Phys. B370 (1992) 310.

[21] ALEPH Collab., D. Buskulic et al., Z. Phys. C62 (1994) 539;
DELPHI Collab., P. Abreu et al., Nucl. Phys. B418 (1994) 403;
L3 Collab., M. Acciarri et al., Z. Phys. C62 (1994) 551.

[22] A. Leike, T. Riemann and J. Rose, Phys. Lett. B273 (1991) 513;
T. Riemann, Phys. Lett. B293 (1992) 451.

[23] S. Kirsch and T. Riemann, Comput. Phys. Commun. 88 (1995) 89.

[24] L3 Collab., O. Adriani et al., Phys. Lett. B315 (1993) 494.

[25] TOPAZ Collab., K. Miyabayashi et al., Phys. Lett. B347 (1995) 171.

[26] G. Isidori, Phys. Lett. B314 (1993) 139.

[27] L3 Collab., M. Acciari et al., *Measurement of Hadron and Lepton-Pair Production at 130 GeV< $\sqrt{s}$ <140 GeV at LEP*, CERN-PPE/95-191.

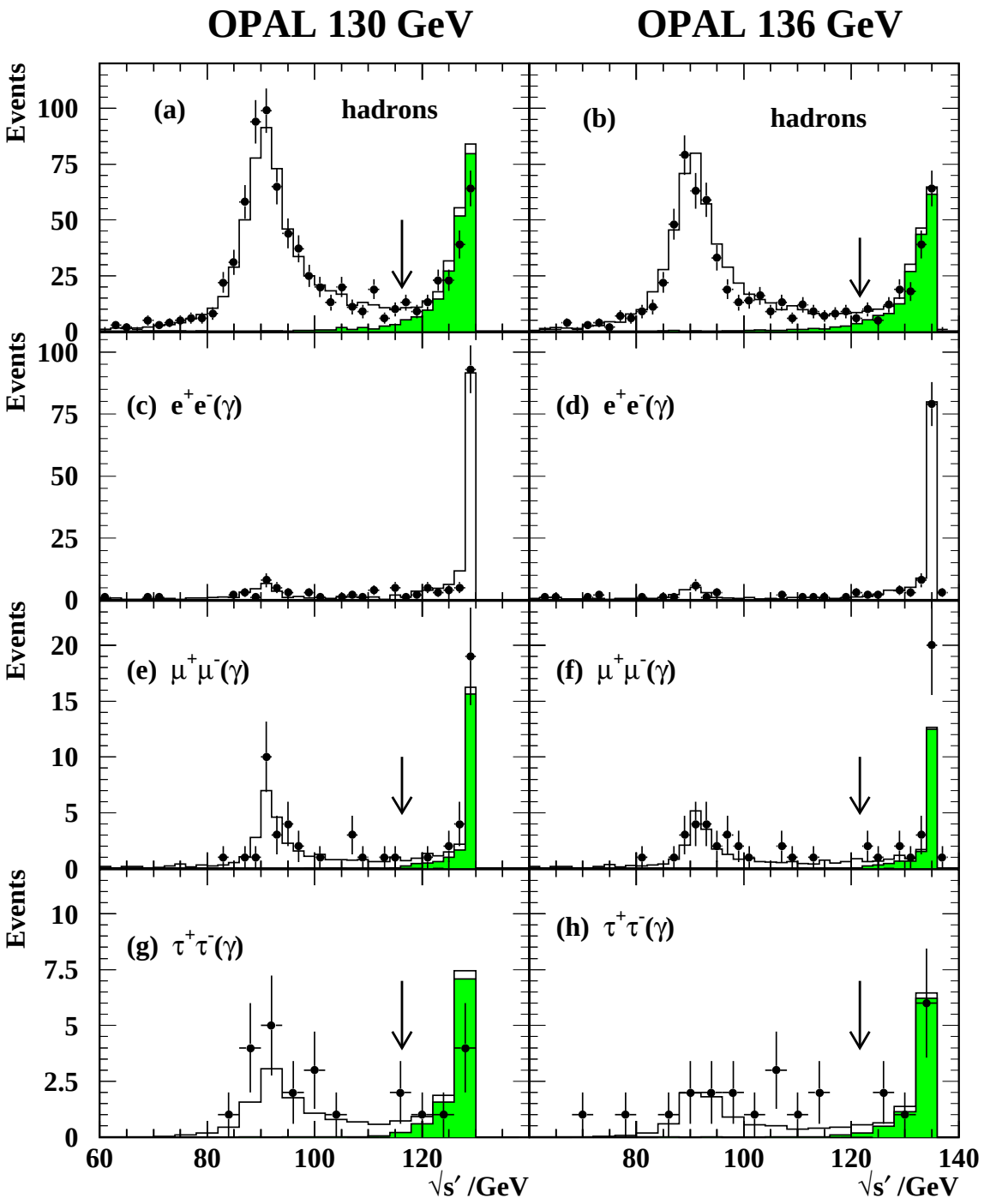

Figure 1: Distributions of $\sqrt{s'}$ at $\sqrt{s}$ = 130 and 136 GeV, for (a) and (b) hadronic events; (c) and (d) electron pair events; (e) and (f) muon pair events; and (g) and (h) tau pair events. The points shown are the data. Open histograms are the predictions of Monte Carlo, including background, with the shaded area, where drawn, representing the prediction for events with $s'/s > 0.8$. The positions of the cuts used to separate non-radiative events are shown by arrows.

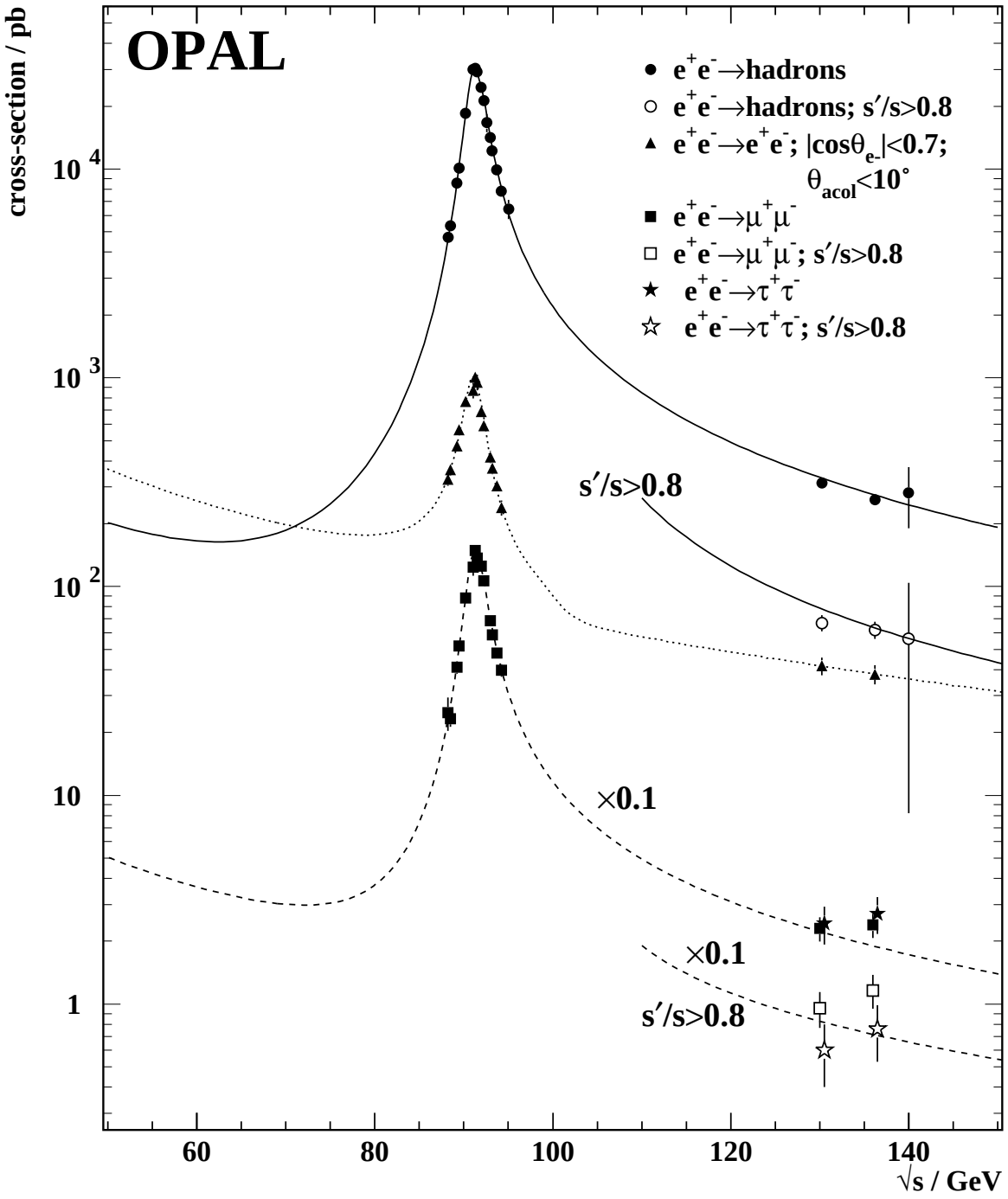

Figure 2: Measured total cross-sections ($s'/s > 0.01$) for different final states from LEP 1 and LEP 1.5 data. The cross-sections for $\mu^+\mu^-$ and $\tau^+\tau^-$ production have been reduced by a factor of ten for clarity. The curves show the predictions of ZFITTER for multihadron (solid) and muon-pair (dashed) final states and that of ALIBABA for the e^+e^- final state (dotted). In the case of multihadrons, muon and tau pairs, cross-section expectations and measurements are shown at high energies also for $s'/s > 0.8$.

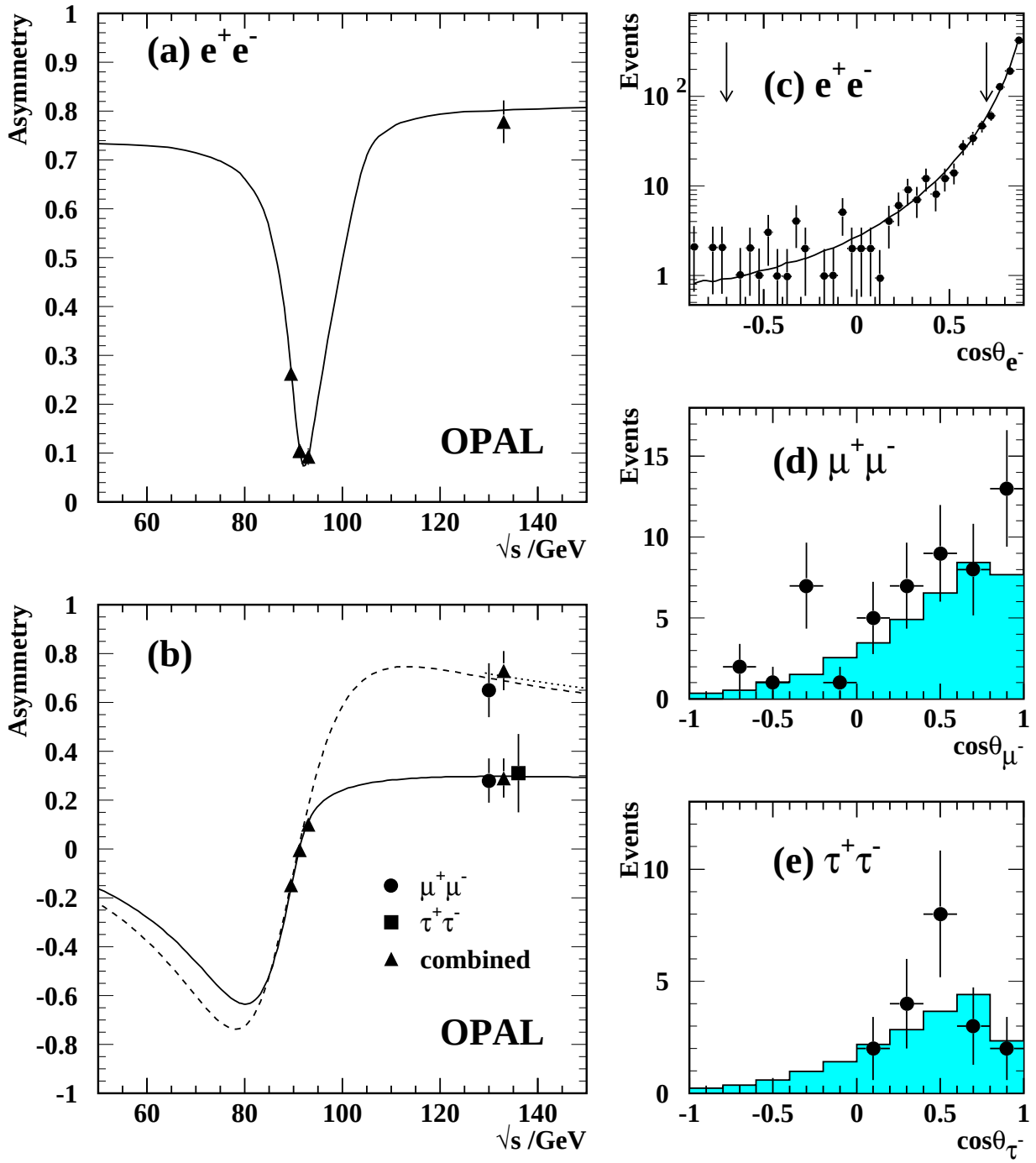

Figure 3: (a) Measured forward-backward asymmetry for electron pairs selected with $|\cos\theta_{e^-}| < 0.7$ and $\theta_{acol} < 10^\circ$, as a function of $\sqrt{s}$. The curve shows the prediction of ALIBABA. (b) Measured asymmetries for all ($s'/s > 0.01$) and non-radiative ($s'/s > 0.8$) samples as functions of $\sqrt{s}$ for $\mu^+\mu^-$ and $\tau^+\tau^-$ events. The measurements are separated horizontally for clarity. The curves show ZFITTER predictions for $s'/s > 0.01$ (solid) and $s'/s > 0.8$ (dotted), as well as the Born-level expectation without QED radiative effects (dashed). The expectation for $s'/s > 0.8$ lies close to the Born curve. The observed distributions of $\cos\theta$ of the outgoing lepton are shown in (c) to (e), for $s'/s > 0.8$ in (d) and (e). The predicted curve in (c) comes from ALIBABA, the histograms in (d) and (e) show the expected distributions from Monte Carlo simulated events. The arrows in (c) show the positions of the cuts at $|\cos\theta_{e^-}| = \pm 0.7$. The high energy data from $\sqrt{s}$ = 130-136 GeV have been combined for this figure.

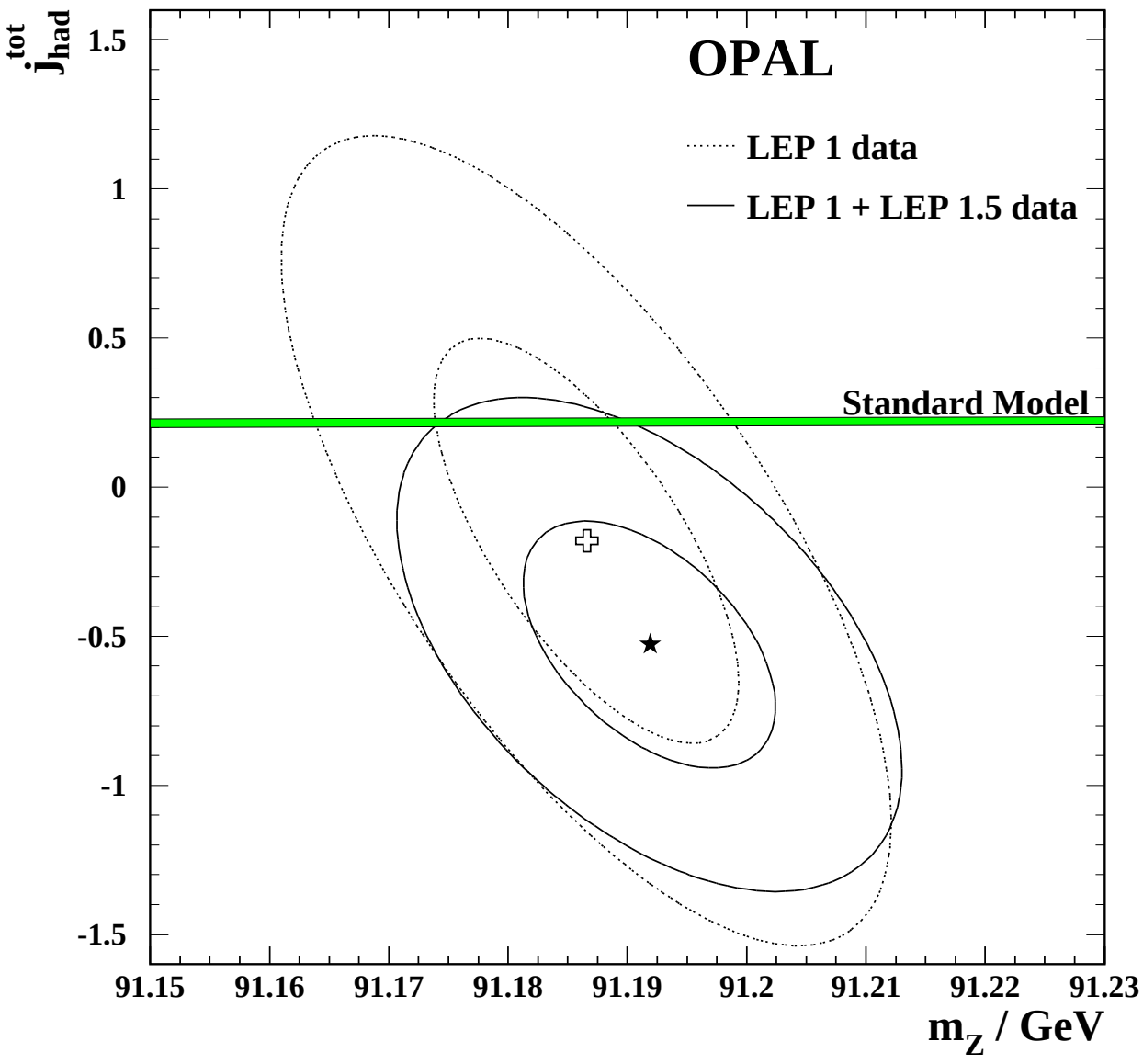

Figure 4: One and two standard deviation (39% and 86% probability content) contours in the j^{tot}_{had} vs. m_Z plane derived from published OPAL LEP 1 data alone (dotted) and including also the higher energy LEP 1.5 data reported here (solid). The central values are shown as a cross and star, respectively. The Standard Model expectation $j^{tot}_{had} = 0.22 \pm 0.02$ (for a top mass range 170-190 GeV and a Higgs mass range of 100-1000 GeV) is shown as the horizontal band.